Applied Clay Science 169 (2019) 67–73

Contents lists available at ScienceDirect

Applied Clay Science

journal homepage: www.elsevier.com/locate/clay

Research Paper

First principles study of structural properties and electric field gradients in kaolinite

Diego Richard[a,b,*], Nicolás M. Rendtorff[a,c]

[a] Facultad de Ciencias Exactas, Universidad Nacional de La Plata (UNLP), 1900 La Plata, Argentina
[b] Instituto de Física La Plata (IFLP), CONICET, CC 67, 1900 La Plata, Argentina
[c] Centro de Tecnología de Recursos Minerales y Cerámica (CETMIC), CIC-CONICET, Camino Centenario y 506, CC 49, B1897ZCA M. B. Gonnet, Argentina

ARTICLE INFO

Keywords:
Kaolinite
DFT
Local structure
Electric field gradients
Hyperfine interactions

ABSTRACT

This work reports a gauge-including projected augmented waves (GIPAW) method study of the structural and electronic properties of kaolinite ($Al_2Si_2O_5(OH)_4$). Different equilibrium structures were determined, and the corresponding electronic density of states and the electric field gradients (EFG) at each atomic site were calculated. The comparison of those predicted properties with measurements that come from neutron powder diffraction, single crystal synchrotron measurements, and nuclear magnetic resonance spectroscopies allowed a detailed study of the structure. In particular, the first principles calculations considered in this work cover different scales, going from the crystallographic structure to the atomic local environments, and serve as a tool to link both the structural and the hyperfine properties. This methodology predictions successfully solves a kaolinite structure in which the atomic local surroundings are consistent with the EFG measurements, thus providing answers to previous controversies between experimental studies about Al and Si local structures and the orientation of OH groups within the structure. In this sense, the GIPAW calculations support that kaolinite consists of asymmetrically distorted Si tetrahedra and Al octahedra sheets, and the interlayer OH groups are oriented nearly perpendicular to the layer.

1. Introduction

Kaolinite is a very common clay mineral which has been studied during almost the last century (Brindley and Robinson, 1945; Keller, 1982). In the last decades many investigations on its structural and electronic properties have been reported, either experimentally (Hayashi et al., 1992; Bish, 1993; Rocha and de Jesus, 1994; Frost et al., 1998; Neder et al., 1999; Lee and Tebbins, 2003; Lee et al., 2003; Zhou et al., 2009; Paris, 2014; Pietzsch et al., 2015; Andrini et al., 2016; Ertan et al., 2017; Fafard et al., 2017) or by first principles (Balan et al., 2001; Sato et al., 2005; Zhou et al., 2009; He et al., 2011; Militzer et al., 2011; Nisar et al., 2011; Chao et al., 2012; Paris, 2014; Pietzsch et al., 2015; Ertan et al., 2017; Fang et al., 2017; Fu and Yang, 2017). This compound is often considered having an almost perfect 1:1 layer structure, which consists of the repetition of a silica sheet where Si atoms are tetrahedrally coordinated by oxygen atoms, and a gibbsite-type sheet in which Al atoms are octahedrally coordinated by oxygen atoms and hydroxyl groups (Brigatti et al., 2006). Kaolinite is the principal phase of the so called kaolinitic clays; the importance of kaolinitic clays in the development of modern ceramic science can best be appreciated by considering its widespread influence on ceramic, material science, and mineralogy (Murray, 1999; Chakraborty, 2016). These clays have been widely used in different technological applications for thousands of years (Schroeder and Erickson, 2014). The majority of the applications include a thermal treatment (Andrini et al., 2016).

According to low-temperature neutron powder diffraction and single crystal X-ray synchrotron measurements, kaolinite belongs to the triclinic system and the space group of symmetry is $C1$ (Bish, 1993; Neder et al., 1999). However, the involved structure refinements are not conclusive in what refers to the local structure of Si and Al atoms. The study by Bish (1993) indicates that both Si tetrahedra and Al octahedra are quite regular, while the results presented by Neder et al. (1999) suggest more distorted cationic environments. At this point, an accurate determination of the regularity of such tetrahedral and octahedral sites is of major importance, considering that the distribution and composition of these sites often determine the surface electronic charge and key structural characteristics, and therefore the properties of the compound which depend on them, such as its reactivity. This controversy about the Si and Al local environments is closely connected

* Corresponding author at: Facultad de Ciencias Exactas, Universidad Nacional de La Plata (UNLP), 1900 La Plata, Argentina.
E-mail address: richard@fisica.unlp.edu.ar (D. Richard).

https://doi.org/10.1016/j.clay.2018.12.013
Received 5 October 2018; Received in revised form 22 November 2018; Accepted 11 December 2018

to the orientation of the hydroxyl groups that link the inner sheets, which remained unclarified until the arrival of calculations based on Density Functional Theory (DFT) (Benco et al., 2001a, 2001b; White et al., 2009; Brigatti et al., 2011). Thus, the *ab initio* methods contribute as a useful tool to unravel experimental issues related to the interpretation of structural and electronic properties of clays materials (White et al., 2009; Smrcok et al., 2010; Brigatti et al., 2011). In this sense, recently, dispersion corrected DFT functionals have been assessed in order to improve the prediction of the structural properties of these materials and relate them with bonding interactions (Tunega et al., 2012; Weck et al., 2015; Fu et al., 2017).

Coming back to the study of the kaolinite bulk structure, an alternative experimental approach to obtain detailed local structural information is by using solid-state nuclear magnetic resonance (NMR) spectroscopies (Hayashi et al., 1992; Rocha and de Jesus, 1994; Lee and Tebbins, 2003; Lee et al., 2003; Zhou et al., 2009; Paris, 2014; Fafard et al., 2017). In particular, the use of these hyperfine techniques with ^{17}O and ^{27}Al isotopes allows the measurement of the quadrupolar coupling constant (C_q), which is proportional to electric field gradient (EFG) at the site of those probe-nuclei. Considering the extreme sensitivity of the EFG tensor to changes in the symmetry of the electronic charge density (due to its r^{-3} dependence from the charge sources), its determination can be used for analyzing small changes of the structure near an atomic site. So, the EFG is a very suited tool for exploring the short range order and the structural environment of the atoms at a nanoscopic scale. Although there exist many NMR measurements on kaolinite, most of them did not determine quantitatively the local structures. In this sense, different authors limited to perform a qualitatively description of the atomic sites in the kaolinite structure by means of NMR spectroscopic methods (Hayashi et al., 1992; Rocha and de Jesus, 1994; Lee and Tebbins, 2003; Zhou et al., 2009). Recently, Paris (2014) presented a new ^{27}Al NMR experiment in order to analyze in detail the hyperfine interactions at Al sites, and could resolve the two inequivalent Al sites of kaolinite. In that case, *ab initio* calculations supported highly accurate experiments, and the author showed that through their combination it can be obtained a detailed interpretation of the Al local structures. This experimental and first principles approach applied to the study of the hyperfine properties had no further application to the other atomic sites of the kaolinite structure. Considering this lack of predictions of the EFG and the availability of ^{17}O NMR measurements from which the EFG can be determined (Lee and Tebbins, 2003), it becomes pertinent to analyze from first principles the O atom environments and to quantitatively correlate the NMR data with the predicted structures and the hydroxyl groups array. In this sense, this work presents a detailed study of the kaolinite structure by means of the gauge-including projector augmented wave (GIPAW) method. This method allows an analysis of the electronic and structural properties of the system, and is especially suited to determine the EFG at each atomic site of the structure (Kresse and Joubert, 1999; Profeta et al., 2003; Charpentier, 2011). The simultaneous comparison of the predicted atomic local structures with the corresponding EFGs, and with the available structural and hyperfine experimental data can be used to reach a deeper understanding of the system structure and its related properties. As it will be shown in the present work, by this combination of first principles predictions with experimental results an unambiguous determination of the kaolinite bulk structure can be obtained, which clarifies previous controversies. In this sense, this is the first time that this kind of comprehensive hyperfine DFT study is presented for this clay mineral.

2. Methods

The initial kaolinite structure was taken from the work of Bish (1993) (COD 9009234) (Gražulis et al., 2012). This structure was determined from Rietveld refinement using neutron powder diffraction, and it is often considered a well-determined structure and used as reference data in many experimental and theoretical studies of kaolinite (Akiba et al., 1997; Hobbs et al., 1997; Neder et al., 1999; Balan et al., 2001; White et al., 2009; Zhou et al., 2009; He et al., 2011; Tunega et al., 2012; Paris, 2014; Weck et al., 2015; Kasprzhitskii et al., 2016). It belongs to space group *C*1, and contains two formula units $Al_2Si_2O_5(OH)_4$ per unit cell, where each formula unit contains two crystallographycally inequivalent Si and Al atoms (Si1 and Si2, and Al1 and Al2, respectively, see Fig. 1). As mentioned earlier, kaolinite bulk structure is composed of a sheet of corner-sharing SiO_4 tetrahedra and a sheet of edge-sharing AlO_6 octahedra, both linked by common apical O atoms (Oa1 and Oa2 in Fig. 1). Each SiO_4 tetrahedron is constructed by a central Si atom surrounded by four O atoms, in which one is a Oa atom and the other three are the basal O atoms (labeled as Ob1, Ob2, and Ob3). On the other hand, each AlO_6 octahedron is composed by a central Al atom and six surrounding O atoms, where two of them are the apical oxygens and the other four are O atoms in hydroxyl groups. One of these OH groups is located inside the layer structure between Al and Si sheets (labeled OHinn in Fig. 1), while the remaining three of them lie at the internal surface of kaolinite (or interlayer, OHint1, OHint2, and OHint3).

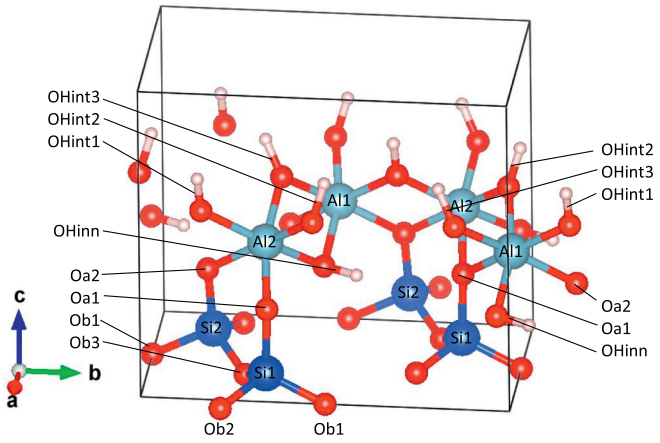

Fig. 1. Kaolinite structure.

First principles calculations were performed within the DFT formalism as implemented in the open-source Quantum ESPRESSO package (Giannozzi et al., 2009). The exchange and correlation energy was assessed by the generalized-gradient approximation as parameterized by Wu and Cohen (2006) (WC-GGA). In addition, the local-density approximation (LDA) was considered (Perdew and Zunger, 1981). The GIPAW pseudopotentials were taken from the library provided by Dal Corso (2014), with the following valence states: Si(3 *s*,3 *p*), Al(3 *s*,3 *p*), O(2 *s*,2 *p*), and H(1 *s*). Converged parameters were obtained using a *k*-space Monkhorst-Pack grid of 4x4x4, and a kinetic energy cutoff of 100 Ry.

As mentioned before, the starting kaolinite structure for the calculations was that experimentally determined by Bish (1993) (called *non-relaxed* in the following). The relevant structural parameters for this investigation, extracted from the work of Bish (1993), are included in Tables 1 and 2. This initial input was optimized until forces in all atoms were lower than 0.001 Ry/Bohr (0.025 eV/Å), according to the Broyden-Fletcher-Goldfarb-Shanno (BFGS) algorithm, and maintaining the unit cell volume fixed at the initial experimental value (*relaxed* structure). This choice of the force tolerance allows a precision on bondlength distances (d_{NN}) within 0.002 Å. Finally, the case of the fully-optimized structure was considered, allowing both atomic positions and cell dimensions relaxation, considering the same force tolerance than before and stress tensor components below 0.5 kbar (*vc-relaxed* structure).

For the three considered structures (*i.e.*, non-relaxed, relaxed, and vc-relaxed) the GIPAW approach was used to determine the EFG tensor

Table 1
Unit cell parameters and Si—O and Al—O bondlengths (d_{NN}) for kaolinite.

	WC-GGA (this work)		Experimental	
	Relaxed	*vc-relaxed*	Bish (1993)	Neder et al. (1999)
a (Å)	5.1535	5.1738	5.1535(3)	5.154(9)
b (Å)	8.9419	8.9850	8.9419(5)	8.942(4)
c (Å)	7.3906	7.3522	7.3906(4)	7.401(10)
α (°)	91.926	91.684	91.926(2)	91.69(9)
β (°)	105.046	105.128	105.046(2)	104.61(5)
γ (°)	89.797	89.755	89.797(2)	89.82(4)
V (Å^3)	328.7	329.8	328.7(1)	329.9
d_{NN} (Å)				
Si1-Oa1	1.613	1.612	1.618(4)	1.614(3)
Si1-Ob1	1.634	1.636	1.611(4)	1.620(3)
Si1-Ob2	1.632	1.633	1.620(4)	1.618(3)
Si1-Ob3	1.639	1.641	1.619(4)	1.628(3)
Si2-Oa2	1.610	1.609	1.612(4)	1.605(3)
Si2-Ob1	1.637	1.639	1.617(4)	1.622(3)
Si2-Ob2	1.631	1.632	1.616(4)	1.616(3)
Si2-Ob3	1.634	1.635	1.608(4)	1.615(3)
Al1-Oa1	1.958	1.963	1.927(6)	1.948(3)
Al1-Oa2	2.021	2.025	1.930(6)	2.001(3)
Al1-OHinn	1.927	1.934	1.913(6)	1.921(3)
Al1-OHint1	1.859	1.860	1.890(6)	1.853(3)
Al1-OHint2	1.850	1.852	1.865(6)	1.849(3)
Al1-OHint3	1.852	1.852	1.915(6)	1.862(3)
Al2-Oa1	2.011	2.015	1.931(6)	1.990(3)
Al2-Oa2	1.946	1.949	1.919(6)	1.946(3)
Al2-Ohinn	1.924	1.931	1.912(5)	1.921(3)
Al2-Ohint1	1.857	1.861	1.896(6)	1.867(3)
Al2-Ohint2	1.856	1.858	1.886(6)	1.858(3)
Al2-Ohint3	1.855	1.856	1.910(6)	1.853(3)

Table 2
Structural parameters for OH groups in kaolinite.

	WC-GGA (this work)		Experimental	
	Relaxed	*vc-relaxed*	Bish (1993)	Neder et al. (1999)
$d_{O\text{-}H}$ (Å)				
Ohinn	0.977	0.976	0.975(4)	0.75
OHint1	0.973	0.973	0.982(4)	0.76(6)
OHint2	0.974	0.975	0.976(4)	0.77(9)
OHint3	0.973	0.974	0.975(4)	0.88(7)
Angle with (001) plane (°)				
Ohinn	0.6	0.4	0.38	12
OHint1	74.3	73.3	73.16	64(4)
OHint2	71.8	70.9	68.24	73(10)
OHint3	63.0	64.1	60.28	47(5)
OHint···O distance (Å)				
OHint1···Ob2	3.013	2.994	3.087(6)	3.088(3)
OHint2···Ob1	2.922	2.903	2.980(7)	2.989(3)
OHint3···Ob3	2.872	2.849	2.945(7)	2.953(3)
OHint···O angle (°)				
OHint1	165.7	164.4	159.6	160(6)
OHint2	161.1	161.4	160.4	173(9)
OHint3	158.6	159.7	154.0	142(5)

at each atomic site (Profeta et al., 2003). This tensor is described by two quantities, its major component in the principal axis system V_{zz}, and the asymmetry parameter $\eta = (V_{xx}\text{-}V_{yy})/V_{zz}$, with V_{ii} the EFG tensor components, ordered according to the convention $|V_{zz}| > |V_{yy}| > |V_{xx}|$. This tensor is related to the measured coupling constant by $C_q = eQV_{zz}/h$, where e is the electron charge, h is Planck's constant, and Q is the nuclear quadrupole moment of the corresponding nuclear sensitive state (Schatz and Weidinger, 1996).

3. Results

3.1. Structure optimization

The structural results after optimizations obtained with the WC-GGA approximation are presented in Table 1. As can be seen, the equilibrium volume determined for the vc-relaxed case slightly overestimates the experimental value in about 0.3%, through an expansion over the *ab* plane and a contraction of the *c* axis. These differences between predicted and experimental values are within the precision range of the DFT methods (Haas et al., 2009; Dal Corso, 2014; Lejaeghere et al., 2014). On the other hand, the d_{NN} values practically do not depend on the choice of the optimization method: differences on d_{NN} values between relaxed and vc-relaxed cells are below 0.5%. Similar results were found with LDA, although in this case the vc-relaxed structure underestimates the experimental volume in about 4%. In the following only the results obtained with the WC-GGA approximation will be analyzed, but it must be noted in advance that the LDA predictions will present, in essence, the same features than the WC-GGA ones. For further details in this respect see supplementary material, where the LDA predictions are provided in extended tables.

The predicted structures seem to be in quite good agreement with the experimental structure determined from low temperature neutron powder diffraction by Bish (1993), being the differences between predicted and experimental d_{NN} values below 5% (see Table 1). However, the predicted d_{NN} distances indicate a significant distortion of Si tetrahedra and Al octahedra. In this sense, in the predicted structures the Si-Oa bonds are about 2% shorter than Si-Ob ones, and Al-Oa and Al-OHinner bonds are 4 to 9% longer than Al-OHint bonds. Considering that the initial structure for the calculations was that of Bish (1993), where Si tetrahedra and Al octahedra are almost regular, the effect of structure optimization is to move the Si and Al atoms towards the interlayer hydroxyl plane. These shifts lead to asymmetrically distorted Si tetrahedra and Al octahedra, and represent a characteristic difference with regard to the starting-point structure. On the other hand, these predicted d_{NN} values are in excellent agreement with those determined from single crystal X-ray measurements of Neder et al. (1999) (see Table 1). In this case, the differences between the calculated and measured d_{NN} values are below 1%, with both d_{NN} sets (predicted and experimental) practically equal in what refers to bondlength ordering for each Si and Al atom. These results suggest that kaolinite bulk structure has distorted Si tetrahedra and Al octahedra sheets. However, the structure determined by Neder et al. (1999) is based on room temperature synchrotron measurements, and it is less reliable for determining the location of H atoms than neutron experiments. So, to gain more insight on this aspect, the structural predictions for the OH groups are presented and compared with the experimental data in Table 2. As can be seen there, relaxed and vc-relaxed cells show practically the same O—H distances ($d_{O\text{-}H} \approx 0.975$ Å). Regarding the orientation of OH groups, the OHinner is oriented parallel to the (001) plane, and the three OHint groups are arranged nearly perpendicular to the layer, thus forming interlayer OHint···Ob hydrogen bonds. These results are in excellent agreement with the experimentally determined values reported by Bish (1993) using neutron diffraction. As can be seen, differences between the predicted and these experimental $d_{O\text{-}H}$ values are within the experimental error, while for the OH orientation angle with the (001) plane the differences are below 7%. Table 2 also includes the corresponding values of Neder et al. (1999), in order to show in that case the experimental difficulties in determining the location of H atoms, as mentioned before. In that case, if the GIPAW predictions are compared to those structural measurements of Neder et al., differences between $d_{O\text{-}H}$ distances are as high as 30% of the experimental values, and differences for the OH orientation angle are even worse. Fig. S1 in the supplementary material is suggested to perform a visual comparison between both experimental and the predicted structure.

Table 3
WC-GGA predictions for the EFG at each atomic site.

Site	Non-relaxed		Relaxed		vc-relaxed		Experimental		
	V_{zz}	η	V_{zz}	η	V_{zz}	η	$\lvert V_{zz}\rvert$	η	Ref.
Si1	−0.68	0.84	−1.29	0.50	−1.34	0.49			
Si2	+0.77	0.97	−1.41	0.38	−1.46	0.39			
Al1	−0.79	0.51	−0.99	0.64	−0.94	0.66	0.96(3)	0.8(1)	Paris (2014)
Al2	+0.50	0.84	−0.84	0.92	−0.79	0.97	0.85(3)	0.9(1)	
Oa	−5.04 /−5.11	0.75/0.77	+5.15/+5.19	1.00	−5.18/−5.19	0.94/0.97	5.5(2)/5.7(2)	0.80(5)	Lee and Tebbins (2003)
Ob	+6.93/+7.94	0.28/0.64	+7.05/+7.63	0.49/0.75	+7.25/ +7.79	0.47/ 0.70	7.2(3)/7.7(3)	0.3(1)/0.4(1)	
Oinn	+11.71	0.61	+11.71	0.47	+11.69	0.48	11.2(6)	0.6(2)	
Oint	+12.51/+13.20	0.55/0.59	+11.65/+12.08	0.63/0.65	+11.48/ +11.96	0.65/0.67	11.2(6)	0.6(2)	
H	+4.90/+5.11	0.06	+5.05/+5.15	0.05	+5.05/+5.14	0.05			

V_{zz} values are in units of 10^{21} V/m^2. For O and H sites each cell contains minimum/maximum value. The oxygen atoms of the OHinn and OHint hydroxyl groups were called Oinn and Oint, respectively. Experimental $\lvert V_{zz}\rvert$ was determined from C_q measurements, using $Q(^{21}\text{Al}, 5/2) = +0.147(1)$ b and $Q(^{17}\text{O}, 5/2) = -0.0256(2)$ b (Stone, 2016). Experimental V_{zz} sign is unknown.

3.2. EFGs

The different structures were considered to explore the EFGs at each atomic site of kaolinite. The predicted V_{zz} and η values for non-relaxed, relaxed, and vc-relaxed structures are presented in Table 3, which also includes the available experimental data for the EFG at Al and O sites. As can be seen, for both inequivalent sites of Si and Al, the structural relaxations produce strong changes on V_{zz} and η. This result shows the high sensitivity of the EFG tensor to small changes on the local environments of these sites. For example, considering the results already presented in Table 1, changes on d_{NN} values below 5% (from non-relaxed to relaxed structures) produce a change of 100% on V_{zz} at silicon sites (see Table 3). In the same sense, although both crystallographically inequivalent Al environments are nearly identical in what refer to their d_{NN} values, the associated EFGs strongly differ from each other. On the other hand, the EFG at O and H sites is less sensitive to the registered structural distortions: for these sites, when the structure is allowed to relax V_{zz} and η vary in about 5% and 30%, respectively (see Table 3). According to the predictions, the EFG practically does not depend on the relaxation procedure for all the atomic sites of the structure (*i.e.*, V_{zz} and η values at each site do not present any significant difference when considering either the relaxed or vc-relaxed cell). Again, this result reflects that the EFG tensor is an extremely local quantity, so for a same set of d_{NN} values at an atomic site, the same EFG is obtained, making the effect of the change on the unit cell dimensions on it practically negligible.

When the calculated EFGs are compared with the experimental results that come from ^{27}Al and ^{17}O solid-state NMR measurements, it is found an excellent agreement of the predictions corresponding to relaxed cells with those experimental EFGs. As can be seen in Table 3, the predicted V_{zz} values in such cases for Al1, Al2, Ob, Oinn, and Oint sites are found to be within the experimental error bars, while for the Oa sites the difference between predicted and measured values are about 7%. On the other hand, for the η parameter it is found a similar behavior. Hence, it is necessary to consider the structural relaxations in order to account for the experimental EFGs, especially for the Al sites. Regarding the O sites, even for the non-relaxed structure the predicted EFGs are in good agreement with the available experimental results at these sites. This suggest that the initial structure (*i.e.*, that determined from neutron diffraction) is good enough in describing the oxygen local structures observed by ^{17}O NMR, probably due to the lower EFG sensitivity already mentioned for this probe. At this point it is worthy to mention that the interpretation of ^{17}O NMR spectra is not trivial, then the predictions for the EFG at the oxygen sites presented in this work provide *ab initio* support to the peak assignment performed by Lee and Tebbins (2003) in their experiments. In particular, first principles predictions for V_{zz} suggest that the C_Q value for the Oinner site should be similar to that of the Oint atoms (see Table 3), which is compatible with the fact that hydroxyl groups are not well resolved in ^{17}O NMR experiments.

So, the excellent agreement between the first principles equilibrium structures and the EFG determinations that come from NMR measurements indicates that the GIPAW approach is a proper method to describe the atomic local environments. In this sense, the poor predictions for the EFG at Al sites in the case of the non-relaxed structure can be attributed to an insufficient precision of the neutron powder diffraction technique (on which that structure is based) to determine the cationic local structures, even at low temperatures, as suggested in Section 3.1.

At this point, it is also worthy of investigation the effect of the H location on the EFG at Oinn and Oint sites. To this purpose, further EFG calculations were performed considering the structure fixed at that of Neder et al. (1999), where the OH groups strongly differ in their internal structure and orientation from that of Bish (1993), and also from those already predicted by first principles in this work (see Table 2). In this case, when considering the structure data of Neder et al. (1999) it is found a reduction on V_{zz} values of about 20% at Oinn and Oint sites, compared to those predictions presented in Table 3 for these sites (for further detail see Table S4 in supplementary material). So, by doing this additional test, the EFGs obtained at the O sites are in worse agreement with the experimental NMR data than those values obtained when considering the first principles equilibrium structures. This demonstrates that the considered synchrotron measurements of Neder fail in the description of the hydroxyl groups.

Therefore, despite the possible limitations of the standard DFT methods in providing accurate unit cell dimensions (Haas et al., 2009; Tunega et al., 2012; Lejaeghere et al., 2014), these results show that the predicted bulk structure of kaolinite does not depend on the choice of either the relaxed or vc-relaxed structures. Consequently, the predicted atomic local environments and EFGs for both structures are practically the same. From the comparison with the available experimental data, it is concluded that the proposed first principles method allows the prediction of structures that are consistent with all the features of the kaolinite bulk structure that could be inferred considering the main strength each experimental technique has separately: the positions of the heavy atoms determined from synchrotron measurements on the single crystal, those of the H atoms obtained with neutron powder diffraction, and the local structures at Al and O sites on which the EFGs determined by NMR strongly depend. In summary, *ab initio* calculations support the picture of a kaolinite bulk structure composed by asymmetrically distorted Si tetrahedra and Al octahedra sheets, and with its interlayer OH groups oriented nearly perpendicular to the layer. These predicted structures (calculated with both WC-GGA and LDA) are provided as supplementary material for further analysis.

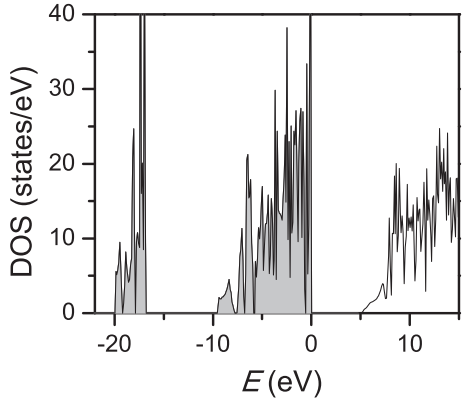

Fig. 2. DOS for vc-relaxed kaolinite structure. Shaded areas indicate occupied energy states.

3.3. Electronic density of states

The density of states (DOS) corresponding to the vc-relaxed cell obtained with the WC-GGA approximation is shown in Fig. 2, where the energy scale refers to the Fermi level. As can be seen, the energy bandgap (E_{gap}) between the valence band (VB) and the conduction band (CB) takes the value 5.1 eV. The VB width is about 10 eV, and is followed by a narrow band at lower energies (from −20 to −17 eV). Similar results were obtained for the relaxed structure (where E_{gap} = 5.3 eV) and also with the LDA approximation (E_{gap} = 4.8 and 5.0 eV for LDA relaxed and vc-relaxed cell, respectively). These predicted bandgap values are consistent with previous first principles calculations (depending on the *ab initio* method, E_{gap} ranges from 4 to 8 eV (Nisar et al., 2011; Chao et al., 2012; Pietzsch et al., 2015)). Experimentally, it has been reported that this energy strongly depends on the defect concentration, so, still, there is not a precise measurement for E_{gap}. However, Pietzsch et al. (2015) speculate that for pristine kaolinite E_{gap} is about 7 eV, and because of the presence of defects it can decrease about 3.2 eV. It is well-known that standard DFT predictions underestimate the experimental E_{gap} values (Perdew, 1985; Mori-Sánchez et al., 2008), but this does not invalidate the fine structure of the DOS and the calculation of quantities which depend only on the ground state as, for example, the EFG and the equilibrium structures (Richard et al., 2013).

In order to gain further insight into the electronic properties of kaolinite, in Fig. 3 the projected density of states (PDOS) by atom and by orbital are presented. It was verified that different atoms under a same label contribute equally to the DOS than those shown in Fig. 3. From the PDOS, it is clear that VB is mainly comprised by O-2*p* states, with slight differences in the contribution to this band depending on the considered oxygen atom. This is a consequence of the different symmetry and position each O atom has in the unit cell. In particular, it can be observed that VB bottom states are due to Ob orbitals, while Oint atoms produce the sharp peak at the top of the VB. From the comparison between the plots of Fig. 3, it is found that the high ionicity of O atoms results in a large charge transfer from Si-3*p*, Al-3*p* and H-1 *s* states to the O-2*p* ones. In addition, there are residual charges in Si and Al orbitals, which imply that it is a minor covalent component in Si—O and Al—O bonds. On the other hand, the band below VB (located around −20 eV, showed in Fig. 2) is mostly due to H-1 *s* and O-2 *s* orbitals. Finally, the CB is composed by *s* and *p* orbitals of all atoms, being the *p* character of Si and Al atoms the most significant near the CB bottom.

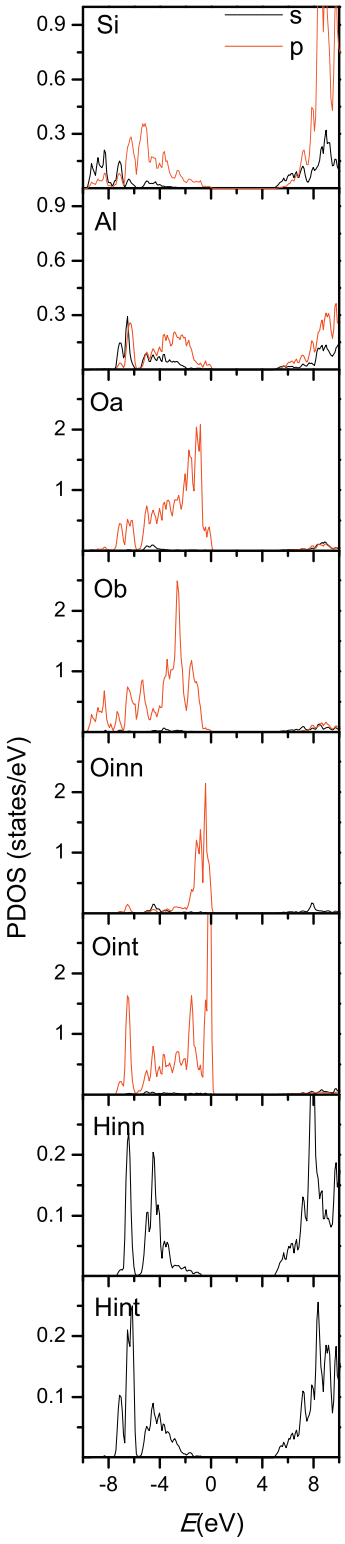

Fig. 3. PDOS for the vc-relaxed structure calculated with the WC-GGA approximation. Different scales were used on the *y* axes to optimize visibility in all graphs. Energies refer to the highest occupied state.

4. Discussion and conclusions

As it was introduced at the beginning of this work, many DFT-based methods have been assessed in the last years in order predict and study different properties of clay materials. For kaolinite, the works of White et al. (2009) and Brigatti et al. (2011) appropriately summarize the state-of-the-art of standard first principles method in studying its structure and related properties. More recently, approaches based on semiempirical methods were implemented in order to predict more

realistically different properties of this system (Tunega et al., 2012; Weck et al., 2015; Castro De Lima et al., 2017; Fu and Yang, 2017; Táborosi et al., 2018). Nevertheless, literature has a lack of information concerning predictions of the EFG at each atomic site of the kaolinite structure, which is a quantity specially suited to study the atomic local structures. In this sense, Zhou et al. (2009) and Paris (2014) reported a brief analysis of the EFG considering standard DFT methods, but only for the aluminium sites and with the purpose of helping to interpret ^{27}Al NMR spectra. So, the present work extended those previous investigations by focusing on the relation of the EFGs with the optimized structures, and using the GIPAW method. In particular, this investigation presented predictions of the EFG for all the atomic sites in the structure. Regarding the atomic structural surroundings for the equilibrium (which are characterized by the d_{NN} values), they adequately fit into the above mentioned *ab initio* background. This work showed also that these surroundings do not depend on the choice of the lattice parameters, *i.e.* if these are those values determined experimentally, or those reached after full structural optimization (relaxed and vc-relaxed cell, respectively). In consequence, predictions for the EFGs are similar for both unit cell dimension sets. Furthermore, those local structures are in very good agreement with previous first principles predictions (Balan et al., 2001; Smrcok et al., 2010; Chao et al., 2012; Weck et al., 2015; Fang et al., 2017; Fu and Yang, 2017), even with those that considered semiempirical corrections to correctly describe the weak interactions involved into the structure (Weck et al., 2015; Tunega et al., 2012; Fu and Yang, 2017; Fu et al., 2017). Considering these agreements, and that the GIPAW method as used in this work involves the open-source Quantum ESPRESSO code, and the recent pseudopotentials by Dal Corso (2014) set for EFG calculations, this *ab initio* method is quite convenient for the considered purposes. On the other hand, when these GIPAW predictions are compared to the experimental data, it is found that the predicted structure overcomes discrepancies between those previously determined from experimental methods, where differences often arose due to relatively high error limits in experimental structures (determined either from neutron powder diffraction or single crystal X-ray diffraction). In this respect, the present investigation demonstrated that the high sensitivity of the EFGs to slight structural changes in the probe surroundings allows a deeper analysis of the kaolinite structure by comparing the GIPAW predictions with NMR measurements.

In summary, this work presented a detailed study of the kaolinite structure from first principles by calculating different equilibrium structures and their corresponding EFGs at each atomic site and their DOS. The agreement between the predicted bulk structures with the available experimental data supports that kaolinite structure has asymmetrically distorted Si tetrahedra and Al octahedra sheets, and that interlayer OH groups are oriented nearly perpendicular to the layer. In this sense, these features of the predicted equilibrium structure are those that can be reached considering the main strengths each of the considered experimental techniques has separately. Hence, GIPAW calculations allowed an unambiguous determination of the kaolinite bulk structure. In addition, it was shown that Si—O and Al—O present a mainly ionic bonding character. This promising approach encourages further investigations on kaolinite-related structures and other clay minerals, which are now underway.

Acknowledgments

This work was supported by: Universidad Nacional de La Plata (under grant “Jóvenes Investigadores”), Consejo Nacional de Investigaciones Científicas y Técnicas (CONICET) and Agencia Nacional de Promoción Científica y Tecnológica (ANPCyT, PICT 2016-1193). The authors thank the computational facilities of the Physics of Impurities in Condensed Matter (PhI) group at IFLP and Departamento de Física (Facultad de Ciencias Exactas, UNLP). Part of the results presented in this work have been obtained by using the facilities of the CCT-Rosario Computational Center, member of the High Performance Computing National System (SNCAD, MincyT-Argentina). The authors are members of CONICET, Argentina.

Appendix A. Supplementary data

Crystal information files (cif), molecular structural data, and experimental details. See doi: https://doi.org/10.1016/j.clay.2018.12.013 contains the supplementary crystallographic data for compound 1. These data can be obtained free of charge from The Cambridge Crystallographic Data Centre *via*http://www.ccdc.cam.ac.uk/data_request/cif. Supplementary data associated with this article can be found in the online version, at https://doi.org/10.1016/j.clay.2018.12.013.

References

Akiba, E., Hayakawa, H., Hayashi, S., Miyawaki, R., Tomura, S., Shibasaki, Y., Izumi, F., Asano, H., Kamiyama, T., 1997. Structure refinement of synthetic deuterated kaolinite by Rietveld analysis using time-of-flight neutron powder diffraction data. Clay Clay Miner. 45, 781–788. https://doi.org/10.1346/CCMN.1997.0450602.

Andrini, L., Gauna, M.R., Conconi, M.S., Suarez, G., Requejo, F.G., Aglietti, E.F., Rendtorff, N.M., 2016. Extended and local structural description of a kaolinitic clay, its fired ceramics and intermediates: an XRD and XANES analysis. Appl. Clay Sci. 124 (125), 39–45. https://doi.org/10.1016/j.clay.2016.01.049.

Balan, E., Saitta, A.M., Mauri, F., Calas, G., 2001. First-principles modeling of the infrared spectrum of kaolinite. Am. Mineral. 86, 1321–1330. https://doi.org/10.2138/am-2001-11-1201.

Benco, L., Tunega, D., Hafner, J., Lischka, H., 2001a. Orientation of OH groups in kaolinite and dickite: Ab initio molecular dynamics study. Am. Mineral. 86, 1057–1065. https://doi.org/10.2138/am-2001-8-912.

Benco, L., Tunega, D., Hafner, J., Lischka, H., 2001b. Upper Limit of the O−H···O Hydrogen Bond. Ab Initio Study of the Kaolinite Structure. J. Phys. Chem. B 105, 10812–10817. https://doi.org/10.1021/jp0124802.

Bish, D.L., 1993. Rietveld refinement of the kaolinite structure at 1.5 K. Clays Clay Miner. 41, 738–744. https://doi.org/10.1346/CCMN.1993.0410613.

Brigatti, M.F., Galan, E., Theng, B.K.G., 2006. Structures and mineralogy of clay minerals. Dev. Clay Sci. 1, 19–86. https://doi.org/10.1016/S1572-4352(05)01002-0.

Brigatti, M.F., Malferrari, D., Laurora, A., Elmi, C., 2011. Structure and mineralogy of layer silicates: recent perspectives and new trends. In: EMU Notes in Mineralogy 11. Vol. 1. pp. 1–71. https://doi.org/10.1180/EMU-notes.11.1.

Brindley, G.W., Robinson, K., 1945. Structure of kaolinite. Nature 156, 661–662. https://doi.org/10.1038/156661b0.

Castro De Lima, F.D., Miwa, R.H., Miranda, C.R., 2017. Retention of contaminants Cd and Hg adsorbed and intercalated in aluminosilicate clays: a first principles study. J. Chem. Phys. 147, 174704. https://doi.org/10.1063/1.5009585.

Chakraborty, A.K., 2016. Phase Transformation of Kaolinite. Springer, New Delhi, India. https://doi.org/10.1007/978-81-322-1154-9. (ISBN 978-81-322-1153-2).

Chao, H.M., Jian, Z., Zhi-Jie, F., 2012. First-principles study of atomic and electronic structures of kaolinite in soft rock. Chin. Phys. B 21, 039101. https://doi.org/10.1088/1674-1056/21/3/039101.

Charpentier, T., 2011. The PAW/GIPAW approach for computing NMR parameters: a new dimension added to NMR study of solids. Solid State Nucl. Magn. Reson. 40, 1–20. https://doi.org/10.1016/j.ssnmr.2011.04.006.

Dal Corso, A., 2014. Pseudopotentials periodic table: from H to Pu. Comput. Mater. Sci. 95, 337–350. https://doi.org/10.1016/j.commatsci.2014.07.043.

Ertan, E., Kimberg, V., Gel'mukhanov, F., Hennies, F., Rubensson, J.E., Schmitt, T., Strocov, V.N., Zhou, K., Iannuzzi, M., Föhlisch, A., Odelius, M., Pietzsch, A., 2017. Theoretical simulations of oxygen K-edge resonant inelastic X-ray scattering of kaolinite. Phys. Rev. B 95, 144301. https://doi.org/10.1103/PhysRevB.95.144301.

Fafard, J., Terskikh, V., Detellier, C., 2017. Solid state 1H and 27Al NMR studies of DMSO-kaolinite intercalates. Clay Clay Miner. 65, 206–219. https://doi.org/10.1346/CCMN.2017.064060.

Fang, Z., Zhai, X., Li, Z., Pan, R., Mo, M., 2017. Pressure dependence of the electronic structure in kaolinite: a first-principles study. Mod. Phys. Lett. B 31, 1750194. https://doi.org/10.1142/S0217984917501949.

Frost, R.L., Tran, T.H., Rintoul, L., Kristof, J., 1998. Raman microscopy of dickite, kaolinite and their intercalates. Analyst 123, 611–616. https://doi.org/10.1039/A707071C.

Fu, L., Yang, H., 2017. Structure and electronic properties of transition metal doped kaolinite nanoclay. Nanoscale Res. Lett. 12, 411. https://doi.org/10.1186/s11671-017-2188-4.

Fu, L., Yang, H., Tang, A., Hu, Y., 2017. Engineering a tubular mesoporous silica nanocontainer with well-preserved clay shell from natural halloysite. Nano Res. 10, 2782–2799. https://doi.org/10.1007/s12274-017-1482-x.

Giannozzi, P., Baroni, S., Bonini, N., Calandra, M., Car, R., Cavazzoni, C., Ceresoli, D., Chiarotti, G.L., Cococcioni, M., Dabo, T., et al., 2009. QUANTUM ESPRESSO: a modular and open-source software project for quantum simulations of materials. J. Phys. Condens. Matter 21, 395502. https://doi.org/10.1088/0953-8984/21/39/395502.

Gražulis, S., Daškevič, A., Merkys, A., Chateigner, D., Lutterotti, L., Quirós, M., Serebryanaya, N.R., Moeck, P., Downs, R.T., Lebail, A., 2012. Crystallography Open

Database (COD): an open-access collection of crystal structures and platform for world-wide collaboration. Nucleic Acids Res. 40, D420–D427. https://doi.org/10.1093/nar/gkr900.
Haas, P., Tran, F., Blaha, P., 2009. Calculation of the lattice constant for solids with semilocal functionals. Phys. Rev. B 79, 085104. https://doi.org/10.1103/PhysRevB.79.085104.
Hayashi, S., Ueda, T., Hayamizu, K., Akiba, E., 1992. NMR Study of Kaolinite. 29SI, 27AI, and 1H Spectra. J. Phys. Chem. 96, 10922–10928. https://doi.org/10.1021/j100205a058.
He, M., Zhao, J., Fang, Z., Zhang, P., 2011. First-principles study of isomorphic ('dual-defect') substitution in kaolinite. Clay Clay Miner. 59, 501–506. https://doi.org/10.1346/CCMN.2011.0590507.
Hobbs, J.D., Cygan, R.T., Nagy, K.L., Schultz, P.A., Sears, M.R., 1997. All-atom ab initio energy minimization of the kaolinite crystal structure. Am. Mineral. 82, 657–662. https://doi.org/10.2138/am-1997-7-801.
Kasprzhitskii, A.S., Lazorenko, G.I., Sulavko, S.N., Yavna, V.A., Kochur, A.G., 2016. A study of the structural and spectral characteristics of free and bound water in kaolinite. Opt. Spectrosc. 121, 357–363. https://doi.org/10.1134/S0030400X16090113.
Keller, W.D., 1982. Kaolin - a most diverse rock in genesis, texture, physical properties, and uses. Geol. Soc. Am. Bull. 93, 27–36. https://doi.org/10.1130/0016-7606(1982)93<27:KMDRIG>2.0.CO;2.
Kresse, G., Joubert, D., 1999. From ultrasoft pseudopotentials to the projector augmented-wave method. Phys. Rev. B 59, 1758. https://doi.org/10.1103/PhysRevB.59.1758.
Lee, S.K., Tebbins, J.F., 2003. O atom sites in natural kaolinite and muscovite: 17O MAS and 3QMAS NMR study. Am. Mineral. 88, 493–500. https://doi.org/10.2138/am-2003-0403.
Lee, S.K., Tebbins, J.F., Weiss, C.A., Kirkpatrick, R.J., 2003. 17O and 27Al 260 5MAS and 3QMAS NMR Study of Synthetic and Natural Layer Silicates. Chem. Mater. 15, 2605–2613. https://doi.org/10.1021/cm030165h.
Lejaeghere, K., Van Speybroeck, V., Van Oost, G., Cottenier, S., 2014. Error estimates for solid-state Density-Functional Theory predictions: an overview by means of the ground-state elemental crystals. Crit. Rev. Solid State Mater. Sci. 39, 1–24. https://doi.org/10.1080/10408436.2013.772503.
Militzer, B., Wenk, H.R., Stackhouse, S., Stixrude, L., 2011. First-principles calculation of the elastic moduli of sheet silicates and their application to shale anisotropy. Am. Mineral. 96, 125–137. https://doi.org/10.2138/am.2011.3558.
Mori-Sánchez, P., Cohen, A.J., Yang, W., 2008. Localization and delocalization errors in Density Functional Theory and implications for band-gap prediction. Phys. Rev. Lett. 100, 146401. https://doi.org/10.1103/PhysRevLett.100.146401.
Murray, H.H., 1999. Applied clay mineralogy today and tomorrow. Clay Miner. 34, 39–49. https://doi.org/10.1180/000985599546055.
Neder, R.B., Burghammer, M., Grasl, T.H., Schulz, H., Bram, M., Fiedler, S., 1999. Refinement of the kaolinite structure from single crystal synchrotron data. Clay Clay Miner. 47, 487–494. https://doi.org/10.1346/CCMN.1999.0470411.
Nisar, J., Arhammar, C., Jamstorp, E., Ahuja, R., 2011. Optical gap and native point defects in kaolinite studied by the GGA-PBE, HSE functional, and GW approaches. Phys. Rev. B 84, 075120. https://doi.org/10.1103/PhysRevB.84.075120.
Paris, M., 2014. The two aluminum sites in the 27Al MAS NMR spectrum of kaolinite: accurate determination of isotropic chemical shifts and quadrupolar interaction parameters. Am. Mineral. 99, 393–400. https://doi.org/10.2138/am.2014.4607.
Perdew, J.P., 1985. Density functional theory and the band gap problem. Int. J. Quantum Chem. Symp. 19, 497. https://doi.org/10.1002/qua.560280846.
Perdew, J.P., Zunger, A., 1981. Self-interaction correction to density-functional approximations for many-electron systems. Phys. Rev. B 23, 5048. https://doi.org/10.1103/PhysRevB.23.5048.
Pietzsch, A., Nisar, J., Jämstorp, E., Gråsjö, J., Arhammar, C., Ahujaf, R., Rubensson, J.E., 2015. Kaolinite: defect defined material properties - a soft X-ray and first principles study of the band gap. J. Electron Spectrosc. Relat. Phenom. 202, 11–15. https://doi.org/10.1016/j.elspec.2015.02.003.
Profeta, M., Mauri, F., Pickard, C.J., 2003. Accurate first principles prediction of 17ONMR parameters in SiO2: assignment of the zeolite ferrierite spectrum. J. Am. Chem. Soc. 125, 541–548. https://doi.org/10.1021/ja027124r.
Richard, D., Muñoz, E.L., Rentería, M., Errico, L.A., Svane, A., Christensen, N.E., 2013. Ab initio LSDA and LSDA + U study of pure and Cd-doped cubic lanthanide sesquioxides. Phys. Rev. B 88, 165206. https://doi.org/10.1103/PhysRevB.88.165206.
Rocha, J., de Jesus, J.D.P., 1994. 27Al satellite transition MAS-NMR spectroscopy of kaolinite. Clay Min. 29, 287–291. https://doi.org/10.1180/claymin.1994.029.2.14.
Sato, H., Ono, K., Johnston, C.T., Yamagishi, A., 2005. First-principles studies on the elastic constants of a 1:1 layered kaolinite mineral. Am. Mineral. 90, 1824–1826. https://doi.org/10.2138/am.2005.1832.
Schatz, G., Weidinger, A., 1996. Nuclear Condensed Matter Physics - Nuclear Methods and Applications. John Wiley & Sons, Chichester, England.
Schroeder, P.A., Erickson, G., 2014. Kaolin: from ancient porcelains to nanocomposites. Elements 10, 177–182. https://doi.org/10.2113/gselements.10.3.177.
Smrcok, L., Tunega, D., Ramirez-Cuesta, A.J., Scholtzová, E., 2010. The combined inelastic neutron scattering and solid state DFT study of hydrogen atoms dynamics in a highly ordered kaolinite. Phys. Chem. Minerals 37, 571–579. https://doi.org/10.1007/s00269-010-0358-3.
Stone, N.J., 2016. Table of nuclear electric quadrupole moments. At. Data Nucl. Data Tables 111–112, 1–28. https://doi.org/10.1016/j.adt.2015.12.002.
Táborosi, A., Szilagyi, R.K., Zsirka, B., Fónagy, O., Horváth, E., Kristóf, J., 2018. Molecular treatment of nano-kaolinite generations. Inorg. Chem. 57 (12), 7151–7167. https://doi.org/10.1021/acs.inorgchem.8b00877.
Tunega, D., Bucko, T., Zaoui, A., 2012. Assessment of ten DFT methods in predicting structures of sheet silicates: importance of dispersion corrections. J. Chem. Phys. 137, 114105. https://doi.org/10.1063/1.4752196.
Weck, P.F., Kim, E., Jové-Colón, C.F., 2015. Relationship between crystal structure and thermo-mechanical properties of kaolinite clay: beyond standard density functional theory. Dalton Trans. 44 (28), 12550–12560. https://doi.org/10.1039/c5dt00590f.
White, C.E., Provis, J.L., Riley, D.P., Kearley, G.J., van Deventer, J.S.J., 2009. What is the structure of kaolinite? Reconciling theory and experiment. J. Phys. Chem. B 113, 6756–6765. https://doi.org/10.1021/jp810448t.
Wu, Z., Cohen, R.E., 2006. More accurate generalized gradient approximation for solids. Phys. Rev. B 73, 235116. https://doi.org/10.1103/PhysRevB.73.235116.
Zhou, B., Sherriff, B.L., Wang, T., 2009. 27Al NMR spectroscopy at multiple magnetic fields and ab initio quantum modeling for kaolinite. Am. Mineral. 94, 865–871. https://doi.org/10.2138/am.2009.3142.